

Invited Review

Recent Development of Relativistic Molecular Theory

Takahito Nakajima^{1,2,*} and Kimihiko Hirao¹

¹ Department of Applied Chemistry, Graduate School of Engineering,
The University of Tokyo, Tokyo 113-8656, Japan

² PRESTO, Japan Science and Technology Agency, 4-1-8 Honcho Kawaguchi,
Saitama 332-0012, Japan

Received September 27, 2004; accepted December 2, 2004

Published online May 6, 2005 © Springer-Verlag 2005

Summary. Today it is common knowledge that relativistic effects are important in the heavy-element chemistry. The continuing development of the relativistic molecular theory is opening up rows of the periodic table that are impossible to treat with the non-relativistic approach. The most straightforward way to treat relativistic effects on heavy-element systems is to use the four-component *Dirac-Hartree-Fock* approach and its electron-correlation methods based on the *Dirac-Coulomb(-Breit)* Hamiltonian. The *Dirac-Hartree-Fock (DHF)* or *Dirac-Kohn-Sham (DKS)* equation with the four-component spinors composed of the large- and small-components demands severe computational efforts to solve, and its applications to molecules including heavy elements have been limited to small- to medium-size systems. Recently, we have developed a very efficient algorithm for the four-component *DHF* and *DKS* approaches. As an alternative approach, several quasi-relativistic approximations have also been proposed instead of explicitly solving the four-component relativistic equation. We have developed the relativistic elimination of small components (RESC) and higher-order *Douglas-Kroll (DK)* Hamiltonians within the framework of the two-component quasi-relativistic approach. The developing four-component relativistic and approximate quasi-relativistic methods have been implemented into a program suite named REL4D.

In this article, we will introduce the efficient relativistic molecular theories to treat heavy-atomic molecular systems accurately *via* the four-component relativistic and the two-component quasi-relativistic approaches. We will also show several chemical applications including heavy-element systems with our relativistic molecular approaches.

Keywords. Relativistic molecular theory; *Dirac-Hartree-Fock*; *Dirac-Kohn-Sham*; RESC; Higher-order DK; REL4D.

1. Introduction

The relativistic effect has been considered as an essential factor to figure out molecular structures, chemical activities, or various properties of heavy-element systems.

* Corresponding author. E-mail: nakajima@qcl.t.u-tokyo.ac.jp

Recently many quantum chemists have dedicated a lot of efforts to the calculation and treatment of the electronic structures of polyatomic systems including heavy elements, which are involved in many interesting chemical and physical phenomena. They still present unique difficulties to the theoretical study. Until recently, the relativistic effect had ever been thought less important for chemical properties because the relativity appears primarily in the core electrons, which had been believed to be unlikely to affect chemically active valence regions dramatically. Recent studies, however, have revealed not only quantitatively but also qualitatively that the relativistic effect plays essential and comprehensive roles in total natures of molecular electronic structures for heavy-element systems. We are nowadays convinced that the relativistic effect is definitely important for the accurate theoretical treatment of heavy-element systems as well as the electron correlation effect.

To treat relativistic effects theoretically, the *Dirac* equation is usually solved rather than the non-relativistic *Schrödinger* equation. The one-electron *Dirac* Hamiltonian is written as Eq. (1) where the constant c is the speed of light, V_{ext} is the external potential, and $\mathbf{p}(= -i\nabla)$ is the momentum operator.

$$H_D = c \boldsymbol{\alpha} \cdot \mathbf{p} + \beta c^2 + V_{\text{ext}} \quad (1)$$

The 4×4 *Dirac* matrices $\boldsymbol{\alpha}$ and β in Eq. (1) are given by Eq. (2) with the 2×2 *Pauli* spin matrices σ_t (Eq. (3)).

$$\alpha_t \equiv \begin{pmatrix} 0_2 & \sigma_t \\ \sigma_t & 0_2 \end{pmatrix}, \quad t = (x, y, z), \quad \beta \equiv \begin{pmatrix} \mathbf{I}_2 & 0_2 \\ 0_2 & -\mathbf{I}_2 \end{pmatrix} \quad (2)$$

$$\sigma_x \equiv \begin{pmatrix} 0 & 1 \\ 1 & 0 \end{pmatrix}, \quad \sigma_y \equiv \begin{pmatrix} 0 & -i \\ i & 0 \end{pmatrix}, \quad \sigma_z \equiv \begin{pmatrix} 1 & 0 \\ 0 & -1 \end{pmatrix} \quad (3)$$

Since the *Dirac* equation is valid only for the one-electron system, the one-electron *Dirac* Hamiltonian has to be extended to the many-electron Hamiltonian in order to treat the chemically interesting many-electron systems. The straightforward way to construct the relativistic many-electron Hamiltonian is to augment the one-electron *Dirac* operator, Eq. (1), with the *Coulomb* or *Breit* (or its approximate *Gaunt*) operator as a two-electron term. This procedure yields the *Dirac-Coulomb* (*DC*) or *Dirac-Coulomb-Breit* (*DCB*) Hamiltonian derived from quantum electrodynamics (QED) (Eq. (4)) where g_{ij}^C and g_{ij}^{CB} are given by Eqs. (5) and (6).

$$H = \sum_i H_D(\mathbf{r}_i) + \sum_{i>j} g_{ij} \quad (4)$$

$$g_{ij}^C = \frac{1}{r_{ij}} \quad (5)$$

$$g_{ij}^{CB} = \frac{1}{r_{ij}} - \frac{1}{2} \left(\frac{(\boldsymbol{\alpha}_i \cdot \boldsymbol{\alpha}_j)}{r_{ij}} + \frac{(\boldsymbol{\alpha}_i \cdot \mathbf{r}_{ij})(\boldsymbol{\alpha}_j \cdot \mathbf{r}_{ij})}{r_{ij}^3} \right) \quad (6)$$

The *DCB* Hamiltonian is covariant to first order, and the presence of the *Breit* (or approximate *Gaunt*) interaction serves to increase the accuracy of calculated spectroscopic splittings and core binding energies.

Historically, approaches to treat the electronic structure relativistically have split into two camps: one is the four-component relativistic approach and another is the two-component one. In this article, focusing on our recent studies, we will introduce these two types of relativistic approaches. The reader is referred to the detailed reviews for our recent works [1–3].

2. Four-Component Relativistic Molecular Theory

2.1. Dirac-Hartree-Fock and Dirac-Kohn-Sham Methods

By an application of an independent-particle approximation with the *DC* or *DCB* Hamiltonian, the similar derivation of the non-relativistic *Hartree-Fock* (*HF*) method and *Kohn-Sham* (*KS*) density functional theory (DFT) yields the four-component *Dirac-Hartree-Fock* (*DHF*) and *Dirac-Kohn-Sham* (*DKS*) methods with large- and small-component spinors.

The matrix *DHF/DKS* equation is generally written as shown by Eq. (7) where \mathbf{c} is a matrix of molecular spinor coefficients, $\boldsymbol{\varepsilon}$ a spinor energy matrix, and \mathbf{S} an overlap matrix (Eq. (8)) with two-component atomic spinors χ_p^L and χ_p^S for large (L) and small (S) components, respectively.

$$\mathbf{F} \mathbf{c} = \boldsymbol{\varepsilon} \mathbf{S} \mathbf{c} \quad (7)$$

$$\mathbf{S}_{pq} = \begin{pmatrix} \mathbf{S}_{pq}^{LL} & 0 \\ 0 & \mathbf{S}_{pq}^{SS} \end{pmatrix} = \begin{pmatrix} \langle \chi_p^L | \chi_q^L \rangle & 0 \\ 0 & \langle \chi_p^S | \chi_q^S \rangle \end{pmatrix} \quad (8)$$

Assuming the *DC* Hamiltonian, the *Fock* matrix \mathbf{F} is given by Eq. (9).

$$\begin{aligned} \mathbf{F}_{pq} &= \begin{pmatrix} \mathbf{F}_{pq}^{LL} & \mathbf{F}_{pq}^{LS} \\ \mathbf{F}_{pq}^{SL} & \mathbf{F}_{pq}^{SS} \end{pmatrix} \\ &= \begin{pmatrix} \mathbf{V}_{pq}^{LL} + \mathbf{J}_{pq}^{LL} - t_{\text{ex}} \mathbf{K}_{pq}^{LL} - t_{\text{xc}} \mathbf{V}_{\text{xc}pq}^{LL} & c \mathbf{\Pi}_{pq}^{LS} - t_{\text{ex}} \mathbf{K}_{pq}^{LS} \\ c \mathbf{\Pi}_{pq}^{SL} - t_{\text{ex}} \mathbf{K}_{pq}^{SL} & \mathbf{V}_{pq}^{SS} - 2c^2 \mathbf{S}_{pq}^{SS} + \mathbf{J}_{pq}^{SS} - t_{\text{ex}} \mathbf{K}_{pq}^{SS} - t_{\text{xc}} \mathbf{V}_{\text{xc}pq}^{SS} \end{pmatrix} \end{aligned} \quad (9)$$

Here, $\mathbf{\Pi}_{pq}^{X\bar{X}}$, \mathbf{V}_{pq}^{XX} , $\mathbf{V}_{\text{xc}pq}^{XX}$, \mathbf{J}_{pq}^{XX} , and \mathbf{K}_{pq}^{XY} ($X, Y = L$ or S , $\bar{L} = S$, and $\bar{S} = L$) are kinetic energy integral, *Coulomb* integral, electron-nuclear attraction integral, exchange-correlation potential, *Coulomb* integral, and exchange integral matrices (Eqs. (10)–(14)), respectively, with the density matrix \mathbf{D}_{sr}^{XY} (Eq. (15)).

$$\mathbf{\Pi}_{pq}^{X\bar{X}} = \langle \chi_p^X | (\boldsymbol{\sigma} \cdot \mathbf{p}) | \chi_q^{\bar{X}} \rangle \quad (10)$$

$$\mathbf{V}_{pq}^{XX} = \langle \chi_p^X | V^{\text{nuc}} | \chi_q^X \rangle \quad (11)$$

$$\mathbf{V}_{\text{xc}pq}^{XX} = \left\langle \chi_p^X \left| \frac{\delta E_{\text{xc}}}{\delta \rho} \right| \chi_q^X \right\rangle \quad (12)$$

$$\mathbf{J}_{pq}^{XX} = \sum_{Y=L,S} \sum_{r,s} \mathbf{D}_{sr}^{YY} \left(\chi_p^X \chi_q^X | \chi_r^Y \chi_s^Y \right) \quad (13)$$

$$\mathbf{K}_{pq}^{XY} = \sum_{r,s} \mathbf{D}_{sr}^{XY} \left(\chi_p^X \chi_s^X | \chi_r^Y \chi_q^Y \right) \quad (14)$$

$$\mathbf{D}_{sr}^{XY} = \sum_i^{N_{\text{occ}}} c_{si}^X c_{ri}^{Y*} \quad (15)$$

The parameter t_{xc} is set to zero and one for the *DHF* and *DKS* approaches, respectively, and the constant t_{ex} is the parameter for the hybrid DFT approach, usually set to zero for the pure DFT approach.

The four-component *DHF/DKS* method is a theoretically straightforward relativistic approach. For heavy atoms four-component basis set expansion calculations are routine and attain spectroscopic accuracy together with extant correlation methods [4, 5]. Recently the molecular *DHF* and *DKS* methods have become familiar and powerful relativistic approaches with the continuous development of efficient computational algorithms using the basis set expansion. Several four-component *ab initio* molecular programs for polyatomics, *e.g.*, MOLFDIR [6], DIRAC [7], BERTHA [8], and others [9–11], have been developed so far. Unfortunately, however, the treatment of more than one heavy atom within a molecule is not yet routine. The bottleneck in four-component calculations on heavy-element systems is evaluation of the two-electron electron repulsion integrals (ERIs). The number of relativistic integrals is greater than that of non-relativistic ones because the kinetic balance [12] between the large- and small-component primitive *Gaussian*-type spinors (*GTSs*) must be incorporated.

We have recently developed an efficient computational scheme for the four-component method that employs four-component contraction for molecular basis spinors and the new atomic spinor (AS) integral algorithm [13–15]. In the following sections we will briefly introduce our new relativistic scheme.

2.2. Generally Contracted *Gaussian*-type Spinors and Kinetic Balance

Accurate treatment of core spinors and of the valence spinors in the core region by a large basis set expansion is necessary, because most major relativistic effects, or the kinematic effects, come from the region near the nuclei. Because the core spinors change little with chemical environment, the extensive basis set contraction is possible. The difficulty in introducing contracted *GTSs* lies in the fact that the kinetic balance condition [12] between the large- and small-component primitive *GTSs* and spin-orbit splitting of spinors must be incorporated.

In our four-component molecular approach, thus, we use spin-coupled, kinetically balanced, generally contracted *Gaussian*-type spinors as basis functions. The basis expansion is given by Eq. (16) where φ_{μ}^{2L} and φ_{μ}^{2S} are two-component basis spinors, and c_{μ}^L and c_{μ}^S are expansion coefficients.

$$\begin{pmatrix} \psi_i^{2L} \\ \psi_i^{2S} \end{pmatrix} = \sum_{\mu}^n \begin{pmatrix} c_{\mu i}^L \varphi_{\mu}^{2L} \\ c_{\mu i}^S \varphi_{\mu}^{2S} \end{pmatrix}, \quad (16)$$

Since both scalar wavefunctions within a two-component basis spinor are multiplied by a common coefficient in Eq. (16), the dimensions of both the large and small components are n and the total number of variational parameters is $2n$. In the pioneering four-component program package, MOLFDIR, as well as in DIRAC, four-spinors are expanded in decoupled scalar spin-orbitals (Eq. (17)).

$$\begin{aligned} \psi_i = & \sum_{\mu}^{n^L} c_{\mu i}^{L\alpha} \varphi_{\mu}^{L\alpha} \begin{pmatrix} 1 \\ 0 \\ 0 \\ 0 \end{pmatrix} + \sum_{\mu}^{n^L} c_{\mu i}^{L\beta} \varphi_{\mu}^{L\beta} \begin{pmatrix} 0 \\ 1 \\ 0 \\ 0 \end{pmatrix} + \sum_{\mu}^{n^S} c_{\mu i}^{S\alpha} \varphi_{\mu}^{S\alpha} \begin{pmatrix} 0 \\ 0 \\ 1 \\ 0 \end{pmatrix} \\ & + \sum_{\mu}^{n^S} c_{\mu i}^{S\beta} \varphi_{\mu}^{S\beta} \begin{pmatrix} 0 \\ 0 \\ 0 \\ 1 \end{pmatrix} \end{aligned} \quad (17)$$

There are $2n^L$ large-component and $2n^S$ small-component basis spinors. Imposing the kinetic balance implies that $2n^S > n = 2n^L$. Our scheme thus reduces the number of functions required for the small component.

The form of the large-component primitive set ψ_k^{2L} is chosen from large-component spinors obtained by analytical solution of the one-electron *Dirac* equation. The small-component set ψ_k^{2S} is derived so that it satisfies the accurate and rigorous kinetic balance condition versus ψ_k^{2L} , Eq. (18), rather than Eq. (19).

$$\psi_k^{2S} = i(V - E - 2c^2)^{-1} (\boldsymbol{\sigma} \cdot \mathbf{p}) \psi_k^{2L} \quad (18)$$

$$\psi_k^{2S} = i(\boldsymbol{\sigma} \cdot \mathbf{p}) \psi_k^{2L} \quad (19)$$

2.3. Efficient Evaluation of Electron Repulsion Integrals

In construction of *Coulomb* and exchange integral matrices (Eqs. (13) and (14)), three types of electron repulsion integrals (ERIs), (LL|LL), (LL|SS) (or (SS|LL)), and (SS|SS), are required within the *Coulomb* approximation to the electron–electron interaction. Evaluation of ERIs includes a scaling with the fourth power of the number of basis functions formally and is the most time-consuming step within the *DHF/DKS* calculation. To evaluate relativistic ERIs efficiently, we have recently developed a new integral evaluation method specialized for relativistic contracted *Gaussian*-type spinors (GTSs) [13, 15]. The algorithm exploits the transfer relation of *Head-Gordon* and *Pople* (*HGP*) [16] and the accompanying coordinate expansion (ACE) formulas derived by *Ishida* [17] in the non-relativistic case. In this method, four-component ERIs (LL|LL), (LL|SS), and (SS|SS) reduce to several common two-center terms using the *HGP* transfer relation. The common integrals are evaluated rapidly using the ACE method.

We have performed comparative calculations of ERIs using MOLFDIR2000 and DIRAC version 3.2 in comparison with our REL4D program. MOLFDIR and DIRAC do not treat separately contracted REL4D-type basis sets. To make direct comparison possible, calculations with REL4D were done with the commonly contracted basis spinors employed in MOLFDIR and DIRAC, although the

Table 1. CPU times (in hours) for computing four-component ERIs for Au₂, where the basis set used for Au is: [19s14p10d5f]/(6s4p3d1f), which is commonly contracted between $A = +$ and $A = -$

	LLLL + LLSS + SSSS	LLLL + LLSS	LLLL
Present ^a	1.37	0.77	0.21
DIRAC ^b	2.09	0.62	0.050
MOLFDIR ^c	76.35	21.16	1.63

^a Number of basis spinors: 160 (for the large and small components); ^b number of basis spinors: 184 (for the large component) and 424 (for the small component); ^c number of basis spinors: 160 (for the large component) and 420 (for the small component)

program is not optimized for such basis sets. Table 1 displays CPU times for computations on Au₂ with the [19s14p10d5f]/(6s4p3d1f) set. REL4D proved fastest for LLLL + LLSS + SSSS. LLLL + LLSS calculations with the present code were comparable to those of DIRAC. In the LLLL calculations, the present code worked about four times slower than DIRAC. Note that the numbers of spinors generated are different for each program: 160 for the large and small components in REL4D; 160 for the large component and 420 for the small component in MOLFDIR; 184 for the large component and 424 for the small component in DIRAC. The slightly larger basis size in DIRAC is caused by the fact that it uses, not spherical harmonic *GT*Ss, but contracted Cartesian *GT*Ss. This feature improves DIRAC's performance in some cases because the transformation from Cartesian to spherical harmonic is omitted. The reduced size of the small component basis renders our computational scheme efficient in storage, computation, and transformation of integrals, and in matrix manipulations.

2.4. Relativistic Pseudospectral Approach

Recently we have proposed more efficient relativistic molecular theory by an application of the pseudospectral (PS) approach [18]. In the PS approach [19, 20], we use the mixed basis function between a grid representation in the physical space and spectral representation in the function space.

In the relativistic PS approach, the *Coulomb* matrix element, Eq. (13), is given by Eq. (18) with the three-center one-electron integral A_{pq}^{XY} (Eq. (19)) and $\rho(g)$ is the electronic density, which is calculated in terms of the density matrix and atomic spinors at a coordinate r_g .

$$\begin{aligned}
 \mathbf{J}_{pq}^{XX} &= \sum_{Y=L,S} \sum_{r,s} \mathbf{D}_{sr}^{YY} (\chi_p^X \chi_q^X | \chi_r^Y \chi_s^Y) \\
 &\cong \sum_g^M w_g A_{pq}^{XX}(g) \sum_Y^{L,S} \left(\sum_r^N \sum_s^N D_{rs}^{YY} \chi_r^{Y*}(g) \chi_s^Y(g) \right) \\
 &\equiv \sum_g^M w_g A_{pq}^{XX}(g) \rho(g) \tag{20}
 \end{aligned}$$

$$A_{pq}^{XY}(g) = \int \chi_p^{X*}(1) \frac{1}{|r_1 - r_g|} \chi_q^Y(1) dr_1 \tag{21}$$

Likewise, the exchange contribution in the relativistic PS approach is given by Eqs. (22) and (23) for diagonal (LL and SS) and non-diagonal (LS and SL) parts in the *DHF* or *DKS* matrix, respectively.

$$\begin{aligned} \mathbf{K}_{pq}^{\text{XX}} &= \sum_{r,s} \mathbf{D}_{sr}^{\text{XX}} (\chi_p^{\text{X}} \chi_s^{\text{X}} | \chi_r^{\text{X}} \chi_q^{\text{X}}) \\ &\cong \sum_g^M w_g \chi_p^{\text{X}*}(g) \left[\sum_r^N \left(\sum_s^N D_{rs}^{\text{XX}} \chi_s^{\text{X}}(g) \right) A_{rq}^{\text{XX}}(g) \right] \end{aligned} \quad (22)$$

$$\begin{aligned} \mathbf{K}_{pq}^{\text{X}\bar{\text{X}}} &= \sum_{r,s} \mathbf{D}_{sr}^{\text{X}\bar{\text{X}}} (\chi_p^{\text{X}} \chi_s^{\text{X}} | \chi_r^{\bar{\text{X}}} \chi_q^{\bar{\text{X}}}) \\ &\cong \sum_g^M w_g \chi_p^{\text{X}*}(g) \left[\sum_r^N \left(\sum_s^N D_{rs}^{\text{X}\bar{\text{X}}} \chi_s^{\text{X}}(g) \right) A_{rq}^{\text{X}\bar{\text{X}}}(g) \right] \end{aligned} \quad (23)$$

We note that no non-diagonal three-center one-electron integral is required in construction of both *Coulomb* and *HF*-exchange matrix elements within the *DC* approximation. Only diagonal $A_{pq}^{\text{LL}}(g)$ and $A_{pq}^{\text{SS}}(g)$ integrals are required. The high efficiency is hence achieved in the relativistic PS approach.

The features of the relativistic PS-*DHF/DKS* method are as follows:

- (1) The computational scaling is reduced from $O(N^4)$ to $O(N^3)$ (N ; the number of basis sets).
- (2) Since the PS evaluation of *HF*-exchange matrix elements as well as *Coulomb* ones is efficient, post *HF* methods and hybrid-type DFT are applicable.
- (3) It is possible to treat the large molecular systems that are compact and three-dimensional with high-quality basis sets in contrast to the fast multipole moment (FMM) method.
- (4) The multigrid technique can powerfully save considerable CPU time in the direct SCF procedure.
- (5) The PS program code is parallelized efficiently because of adoption of the numerical grid partition.
- (6) It is possible to obtain the numerical result with arbitrary accuracy at adequate CPU time by careful choice of the number of grid points.

Table 2 shows the spectroscopic constants and total energies of the gold dimer calculated with the relativistic PS-DFT method using three types of grids. The details of computations are given in Ref. [18]. The results obtained by the conventional DFT method with the analytical ERIs and the experimental data [21, 22] are also listed for comparison. The PS results for spectroscopic constants and total energies become closer to the analytical results as the level of grids is improved. The relativistic PS-DFT method with the ultrafine grid, the highest level of grid sets in this study, gives excellent good agreement with the analytical result. For the equilibrium bond length and the harmonic frequency for Au_2 , the deviation of the ultrafine PS result from the analytical one is negligibly small. The discrepancies of the dissociation energy and the total energy between ultrafine PS and analytical results are $\Delta D_e = -0.4 \text{ eV}$ and $\Delta E = 0.0098 \text{ au}$, respectively. It is also found that the fine grid yields satisfactory results; the difference of the equilibrium bond length, the harmonic frequency, the dissociation energy, and the total energy

Table 2. Spectroscopic constants of the Au dimer calculated by conventional DFT and PS-DFT (B3LYP)

	Analytical	PS (medium) ^a	PS (fine) ^b	PS (ultra) ^c	Exptl.
$R_e/\text{\AA}$	2.554	2.526	2.549	2.554	2.472
ω_e/cm^{-1}	168	191	169	168	191
D_e/eV	1.98	2.11	2.01	1.94	2.36
Energy/au ^d	-.7302	-.8075	-.7678	-.7400	-
Time/s ^e	17497	927	1352	1979	-

^a Medium grid: $50 \times 110 = 5500/\text{atom}$; ^b fine grid: $75 \times 194 = 14550/\text{atom}$; ^c ultrafine grid: $96 \times 302 = 28992/\text{atom}$; ^d total DFT energy, -38096 au; ^e average CPU time per one cycle for the direct SCF step in the DFT calculation including the ERI evaluation, the KS matrix construction, and the SCF diagonalization

between fine PS and analytical results are $\Delta R_e = 0.005 \text{ \AA}$, $\Delta \omega_e = 1 \text{ cm}^{-1}$, $\Delta D_e = 0.3 \text{ eV}$, and $\Delta E = 0.0376 \text{ au}$, respectively.

The multigrid technique can be used in the SCF procedure of present PS calculations. This technique realizes the faster SCF calculation with the PS method. Average CPU times per one cycle for the direct SCF step in the DFT calculation including the ERI evaluation, the KS matrix construction, and the SCF diagonalization are also listed in Table 2. These times are taken from each single-point calculation at $R = 4.8 \text{ au}$. In the present multigrid calculation, the coarse and medium grids are used in the first and second SCF stages, respectively. By adoption of the multigrid approach in this system, the PS methods with medium, fine, and ultrafine grids are 19, 13, and 9 times faster than the traditional analytical method, respectively.

Later PS applications to molecular systems (Sec. 4.2) also show that the relativistic PS-*DHF/DKS* approach is more efficient than the traditional approach without a loss of accuracy.

3. Two-Component Relativistic Molecular Theory

3.1. Approximate Relativistic Hamiltonians

Despite recent implementations of an efficient algorithm for the four-component relativistic approach, the *DC(B)* equation with the four-component spinors composed of the large (upper) and small (lower) components still demands severe computational efforts to solve, and its applications to molecules are currently limited to small- to medium-size systems. As an alternative approach, several two-component quasi-relativistic approximations have been proposed and applied to chemically interesting systems containing heavy elements, instead of explicitly solving the four-component relativistic equation.

An approximate relativistic Hamiltonian should include the following desirable features:

- (1) It should be accurate enough to give a close result to the one-electron *Dirac* or many-electron *Dirac-Coulomb(-Breit)* Hamiltonian.
- (2) It should be efficient and effective to apply to large molecular systems containing heavy elements.

- (3) It should be well balanced so as to describe molecular systems containing a wide variety of atoms in the periodic table with the same quality.
- (4) It should be variationally stable in order to avoid variational collapse in the sense that at least the non-relativistic limit is obtained correctly.
- (5) It should be variational and not perturbative in order to evaluate various energy values and one-electron properties.

The *Breit-Pauli (BP)* approximation [23] is obtained truncating the *Taylor* expansion of the *Foldy-Wouthuysen (FW)* transformed *Dirac* Hamiltonian [24] up to the $(p/mc)^2$ term. The *BP* equation has the well-known mass-velocity, *Darwin*, and spin-orbit operators. Although the *BP* equation gives reasonable results in the first-order perturbation calculation, it cannot be used in the variational treatment.

One of the shortcomings of the *BP* approach is that the expansion in $(p/mc)^2$ is not justified in the case where the electronic momentum is too large, *e.g.*, for a *Coulomb*-like potential. The zeroth-order regular approximation (*ZORA*) [25, 26] can avoid this disadvantage by expanding in $E/(2mc^2 - V)$ up to the first order. The *ZORA* Hamiltonian is variationally stable. However, the Hamiltonian obtained by a higher-order expansion has to be treated perturbatively, similarly to the *BP* Hamiltonian. Other quasi-relativistic methods have been proposed by *Kutzelnigg* [27, 28] and *Dyall* [29].

We have developed two quasi-relativistic approaches. One is the *RESC* method [30–32], and the other is the higher-order *Douglas-Kroll (DK)* method [33–35]. In the following sections we will introduce *RESC* and higher-order *DK* methods briefly.

3.2. *RESC Method*

The *Dirac* equation is equivalent to the Schrödinger-Pauli type equation composed of only the large component (Eq. (24a)) with the normalization condition (Eq. (24b)).

$$\left[V + (\boldsymbol{\sigma} \cdot \mathbf{p}) \frac{c^2}{2mc^2 - (V - E)} (\boldsymbol{\sigma} \cdot \mathbf{p}) \right] \Psi^L = E\Psi^L \quad (24a)$$

$$\langle \Psi^L | 1 + X^\dagger X | \Psi^L \rangle = 1 \quad (24b)$$

Here the *X* operator is defined by Eq. (25).

$$X \equiv [2mc^2 - (V - E)]^{-1} c(\boldsymbol{\sigma} \cdot \mathbf{p}) \quad (25)$$

If Eq. (24a) could be solved with Eq. (24b), the solution to the *Dirac* equation can be obtained exactly. However, Eq. (24a) has the total and potential energies in the denominator, and an appropriate approximation is needed. In our strategy, $E - V$ in the denominator is replaced by the classical relativistic kinetic energy (relativistic substitutive correction) (Eq. (26)).

$$T = (m^2c^4 + p^2c^2)^{1/2} - mc^2 \quad (26)$$

This simple approach is referred to as the relativistic scheme by eliminating small components (RESC). The derivation and the form of the RESC Hamiltonian are given in Ref. [30]. The RESC approach has several advantages. It is variationally stable. It can easily be incorporated in non-relativistic *ab initio* programs, and relativistic effects are considered on the same footing with electron correlation. RESC works well for a number of systems, and recent studies have shown it to give results similar to the *Douglas-Kroll-Hess* (DKH) method for chemical properties, although very large exponents in the basis set can lead to variational collapse in the current RESC approximation, which includes only the lowest truncation of the kinematic operator.

3.3. Douglas-Kroll Method

The *Douglas-Kroll* (DK) approach [36] can decouple the large and small components of the *Dirac* spinors in the presence of an external potential by repeating several unitary transformations. The DK transformation is a variant of the *FW* transformation [24] and adopts the external potential V_{ext} as an expansion parameter instead of the speed of light, c , in the *FW* transformation. The DK transformation correct to second order in the external potential (DK2) has been extensively studied by *Hess* and co-workers [37], and has become one of the most familiar quasi-relativistic approaches. Recently, we have proposed the higher-order DK method and applied the third-order DK (DK3) method to several systems containing heavy elements.

The first step in the DK transformation consists of a free-particle *FW* transformation to the *Dirac* Hamiltonian with the external potential, V_{ext} (Eq. (27)) in momentum space.

$$H_D = \begin{pmatrix} V_{\text{ext}} + c^2 & c\boldsymbol{\sigma} \cdot \mathbf{p} \\ c\boldsymbol{\sigma} \cdot \mathbf{p} & V_{\text{ext}} - c^2 \end{pmatrix} \quad (27)$$

The resulting Hamiltonian yields the free-particle *FW* Hamiltonian and is also referred to as the first-order DK Hamiltonian. In successive DK transformations, in order to remove odd terms of arbitrary order in the external potential, the unitary operator defined by *Douglas* and *Kroll* (Eq. (28)) [36] or the exponential-type unitary operator (Eq. (29)) [33] is employed sequentially.

$$U_n = (1 + W_n^2)^{1/2} + W_n \quad (28)$$

$$U_n = \exp(W_n) \quad (29)$$

Here W_n is an anti-*Hermitian* operator of n -th order in V_{ext} . The resultant DK Hamiltonian is still a four-component formalism. Its two-component reduction is achieved by replacing β by the unit matrix and $\boldsymbol{\alpha}$ by the 2×2 *Pauli* spin matrix $\boldsymbol{\sigma}$. In order to correspond to the non-relativistic limit, the resulting two-component Hamiltonian is shifted by $-2c^2$.

The first-order, second-order, and third-order DK (DK1, DK2, and DK3) Hamiltonians in the two-component form are given as Eqs. (30)–(32) with E_p , E_1 , and W_1

being given by Eqs. (33)–(35) where the kinematical A and R operators and the v operator are defined by Eqs. (36)–(38) and $[a, b]_+$ and $[a, b]$ denote the anti-commutator and the commutator, respectively.

$$H_{DK1} = E_p - c^2 + E_1 \quad (30)$$

$$H_{DK2} = H_{DK1} - \frac{1}{2} \left[W_1, [W_1, E_p]_+ \right]_+ \quad (31)$$

$$H_{DK3} = H_{DK2} + \frac{1}{2} [W_1, [W_1, E_1]] \quad (32)$$

$$E_p = c \left[(\boldsymbol{\sigma} \cdot \mathbf{p})^2 + c^2 \right]^{1/2} \quad (33)$$

$$E_1 = A(V_{\text{ext}} + RV_{\text{ext}}R)A \quad (34)$$

$$W_1 = A(Rv - vR)A \quad (35)$$

$$A = \left(\frac{E_p + c^2}{2E_p} \right)^{1/2} \quad (36)$$

$$R = \frac{c\boldsymbol{\sigma} \cdot \mathbf{p}}{E_p + c^2} \quad (37)$$

$$v(p, p') = \frac{V_{\text{ext}}(p, p')}{E_p + E_{p'}} \quad (38)$$

3.4. Extended Douglas-Kroll Transformations Applied to the Relativistic Many-Electron Hamiltonian

The DK approach satisfies all of the criteria in Section 3.1: the DK transformation avoids the high singularity in the FW transformation by adoption of the external potential as an expansion parameter, and thus the DK Hamiltonian is variationally stable. The DK Hamiltonian can be applied to the variational calculation in contrast to the *Breit-Pauli* Hamiltonian. Criterion (1) is also satisfied by the higher-order DK method for the one-electron system. The $DK3$ Hamiltonian was shown to give excellent agreement with the one-electron *Dirac* Hamiltonian [33].

By an application of the DK transformation to the relativistic many-electron Hamiltonian, recently, we have shown that the many-electron DK Hamiltonian also gives satisfactory results for a wide variety of atoms and molecules compared with the $DC(B)$ Hamiltonian [35]. To consider the higher-order DK transformation to the two-electron interaction, the present approach adopts the effective one-electron potential in the DHF/DKS operator as an expansion parameter in the DK transformation.

The *DHF/DKS* operator, Eq. (9), can be written in the same form to the one-electron *Dirac* Hamiltonian, Eq. (27), by the following replacements (Eqs. (39) and (40)).

$$V_{\text{nuc}} + J^{\text{LL}} + J^{\text{SS}} - t_{\text{ex}}K^{\text{XX}} - t_{\text{xc}}V_{\text{xc}} \rightarrow V_{\text{ext}} \quad (39)$$

$$\boldsymbol{\sigma} \cdot \mathbf{p} - \frac{t_{\text{ex}}}{c}K^{\text{XY}} \rightarrow \boldsymbol{\sigma} \cdot \mathbf{p} \quad (40)$$

By substituting these relations into Eqs. (30)–(38), we can straightforwardly obtain the *DKn-Fock* operators with the *DK* transformation to the *DHF/DKS* potential in the two-component *DKn-HF/KS* equation (Eq. (41)) where ψ_i is the (orthonormalized) two-component *DKn* spinor and ε_i is its spinor energy. The first-order *DK* (*DK1*) operator is given by Eq. (42) with E_0 and E_1 being given by Eqs. (43) and (44) where the A and R^{XY} operators are defined by Eqs. (45) and (46).

$$F_{\text{DKn}}\psi_i = \varepsilon_i\psi_i \quad (41)$$

$$F_{\text{DK1}} = E_0 - c^2 + E_1 \quad (42)$$

$$E_0 = c \left[\left(\boldsymbol{\sigma} \cdot \mathbf{p} - \frac{t_{\text{ex}}}{c}K^{\text{LS}} \right) \left(\boldsymbol{\sigma} \cdot \mathbf{p} - \frac{t_{\text{ex}}}{c}K^{\text{SL}} \right) + c^2 \right]^{1/2} \quad (43)$$

$$E_1 = A(V_{\text{nuc}} + J^{\text{LL}} + J^{\text{SS}} - t_{\text{ex}}K^{\text{LL}} - t_{\text{xc}}V_{\text{xc}})A + AR^{\text{LS}}(V_{\text{nuc}} + J^{\text{LL}} + J^{\text{SS}} - t_{\text{ex}}K^{\text{SS}} - t_{\text{xc}}V_{\text{xc}})R^{\text{SL}}A \quad (44)$$

$$A = \left(\frac{E_0 + c^2}{2E_0} \right)^{1/2} \quad (45)$$

$$R^{\text{XY}} = \frac{c}{E_0 + c^2} \left(\boldsymbol{\sigma} \cdot \mathbf{p} - \frac{t_{\text{ex}}}{c}K^{\text{XY}} \right) \quad (46)$$

In this approach, the density matrix is evaluated self-consistently with both the large and small component spinors, φ_i^{L} and φ_i^{S} , which can be reconstructed from the free-particle *FW* spinors ψ_i in the *Schrödinger* picture (Eqs. (47) and (48)).

$$\varphi_i^{\text{L}} = A\psi_i \quad (47)$$

$$\varphi_i^{\text{S}} = R^{\text{SL}}A\psi_i \quad (48)$$

It is easy to verify that the *DK1* operator, Eq. (42), is equivalent to the *Fock* operator derived from the no-pair or free-particle *FW* Hamiltonian. Likewise, the higher-order *DK* operators are also derived straightforwardly by repeating the *DK* transformations, though their formulae are omitted only because of their lengthy forms.

As molecular applications of the extended *DK* approach, we have calculated the spectroscopic constants for At_2 : equilibrium bond lengths (R_e), harmonic frequencies (ω_e), rotational constants (B_e), and dissociation energies (D_e). A strong spin-orbit effect is expected for these properties because the outer p orbital participates in their molecular bonds. Electron correlation effects were treated by the hybrid

Table 3. Bond lengths (R_e), harmonic frequencies (ω_e), rotational constants (B_e), dissociation energies (D_e), and total energies (E_{tot}) in the equilibrium geometry of At_2 with B3LYP

Hamiltonian	$\frac{R_e}{\text{\AA}}$	$\frac{\omega_e}{\text{cm}^{-1}}$	$\frac{B_e}{\text{cm}^{-1}}$	$\frac{D_e}{\text{eV}}$	$\frac{E_{\text{tot}}}{\text{au}}$
<i>DKS</i>	3.1121	102.0	0.0166	0.542	-45838.2314
<i>DK3-DK3</i>	3.1102	102.3	0.0166	0.546	-45841.9720
<i>DK3-DK3</i> (no mod. V_{xc}) ^a	3.1080	102.3	0.0166	0.552	-45849.7971
<i>DK3-DK2</i>	3.1108	102.3	0.0166	0.545	-45842.2586
<i>DK3-DK1</i>	3.1074	102.6	0.0166	0.552	-45839.6417
<i>DK3-NR</i>	3.1697	95.5	0.0160	0.429	-45849.7240
<i>DK2-DK2</i>	3.1013	103.0	0.0167	0.561	-45773.7217

^a Results without the relativistic modification to V_{xc}

DFT approach with the B3LYP functional. Since several approximations to both the one-electron and two-electron parts of the *DK* Hamiltonian are available, we define that the *DKn1 + DKn2* Hamiltonian ($n1, n2 = 1-3$) denotes the *DK* Hamiltonian with *DKn1* and *DKn2* transformations for the one-electron and two-electron parts, respectively. The *DKn1 + DK1* Hamiltonian is equivalent to the no-pair *DKn1* Hamiltonian. For the two-electron part the electron–electron *Coulomb* operator in the non-relativistic form can also be adopted. The *DKn1* Hamiltonian with the non-relativistic *Coulomb* operator is denoted by the *DKn1 + NR* Hamiltonian.

Table 3 shows the results for At_2 obtained by approximate *DK* schemes in comparison with four-component *DKS* results. The *DK* results for the spectroscopic constants and the total energy in the equilibrium geometry (E_{tot}) become closer to the *DKS* results as the level of theory is improved. The highest level of theory, *DK3-DK3*, as well as *DK3-DK2*, gives fairly good agreement with the four-component result for At_2 . The *DK3-DK3* operator yields $R_e = 3.1102 \text{ \AA}$, $\omega_e = 102.3 \text{ cm}^{-1}$, and $D_e = 0.546 \text{ eV}$, the corresponding four-component *DKS* values being $R_e = 3.1121 \text{ \AA}$, $\omega_e = 102.0 \text{ cm}^{-1}$, and $D_e = 0.542 \text{ eV}$. The discrepancy between *DK3-DK3* and *DKS* Hamiltonians is $\Delta R_e = 0.0019 \text{ \AA}$, $\Delta \omega_e = 0.3 \text{ cm}^{-1}$, and $\Delta D_e = 0.004 \text{ eV}$.

By comparison between the *DK3-DK3* and *DK3-NR* results, it can be seen that two-electron relativistic effects are comparatively large, especially in the dimer; the bond length decreases by 0.06 \AA , the frequency increases by 7 cm^{-1} , the rotational constant increases by 0.0006 cm^{-1} , and the dissociation energy increases by 0.12 eV . Neglect of the relativistic correction to the electron–electron interaction yields inferior results and gives relatively large deviations from the *DK3-DK3* or *DKS* result. It is interesting that the importance of the two-electron *DK* correction for the bond length is shown, because it has been believed so far that the bond length is scarcely affected by the relativistic correction to the electron–electron interaction, while the harmonic frequency and the dissociation energy are often influenced.

The first-order *DK* correction to the electron–electron interaction is satisfactory also in molecular systems, as well as the atomic case. The deviation of *DK3-DK1* from *DK3-DK3* is $\Delta R_e = 0.0028 \text{ \AA}$, $\Delta \omega_e = 0.3 \text{ cm}^{-1}$, and $\Delta D_e = 0.006 \text{ eV}$ for At_2 .

In the DFT approach with our general *DK* transformation, the exchange-correlation potential, V_{xc} , is corrected relativistically. The effect on the *DK* transformation to the exchange-correlation potential was estimated by comparison with the result without the relativistic modification to V_{xc} [(no mod. V_{xc}) in Table 3]. Compared with the full *DK3–DK3* approach, neglect of the relativistic *DK* correction to the exchange-correlation potential hardly affects the calculated spectroscopic values; its effect merely contributes 0.002 Å for R_e and 0.006 eV for D_e and does not affect ω_e and B_e for the At dimer. Thus, it is found that the relativistic correction to the electron–electron interaction contributes mainly to the *Coulomb* potential, not to the exchange-correlation potential.

In consequence, the several numerical results including the present results show that the third-order *DK* transformation to both one-electron and two-electron Hamiltonians gives excellent agreement with the four-component relativistic approach. The first-order *DK* correction to the two-electron interaction is shown to be satisfactory for both atomic and molecular systems.

4. Applications

4.1. Relativistic Effects on Transition Metal Hydroxides. *CuOH*, *AgOH*, and *AuOH*

The study of water on transition metal complexes and surfaces is important in various fields, *e.g.*, corrosion, catalysis, and electrochemistry. The hydroxyl (OH) group has been frequently observed as a result of activation on these systems and the formation of a metal-OH bond is often implicated. A transition metal hydroxide is the simplest model for the interaction of OH on the transition metal system. Thus, the study of transition metal hydroxides provides useful information for the formation of the transition metal-OH bond and the dissociation mechanism of water on the transition metal surface.

Linearity or nonlinearity of the metal hydroxides depends on a balance between ionic and covalent character of the metal-OH bond. Spectroscopic studies indicate that most alkali and alkali earth hydroxides are linear. Recently, *Whitham, Ozeki, and Saito* [38] have studied the pure rotational spectra of *CuOH* and *AgOH*, and reported that both molecules are strongly bent, indicating considerable covalent character of the metal-OH bond.

We investigated the transition metal hydroxides *CuOH*, *AgOH*, and *AuOH* by using the third-order *Douglas-Kroll* method [39]. Electron correlation effects are also fully taken into account. To the best of our knowledge, there have been no previous experimental and theoretical studies of *AuOH*, for which the relativistic effect is expected to be more significant than for *CuOH* and *AgOH*.

The calculated equilibrium geometries (R_{MO} , R_{OH} , and θ_{MOH}) and dissociation energies (D_e) of *CuOH*, *AgOH*, and *AuOH* are presented in Table 4. The available experimental data [38] of *CuOH* and *AgOH* are also listed for comparison.

For *CuOH*, the electron correlation is larger than the relativistic effect. The electron correlation effect decreases the Cu–OH bond and increases the O–H bond length. In addition, the electron correlation considerably reduces the *CuOH* bond angle. The large increase of the dissociation energy is also due to the electron

Table 4. Bond lengths (R_e), bond angles (θ), and dissociation energies (D_e) in the equilibrium geometry of CuOH, AgOH, and AuOH calculated by the nonrelativistic (NR) and relativistic (DK3) methods

Method	$R_{MO}/\text{\AA}$	$R_{OH}/\text{\AA}$	θ_{MOH}/deg	D_e/eV
CuOH				
NR-SCF	1.846	0.943	119.4	1.59
NR-CCSD(T)	1.799	0.973	109.2	3.05
DK3-SCF	1.826	0.943	117.8	1.59
DK3-CCSD(T)	1.774	0.974	108.1	3.08
Exptl. ^a	1.774182(3)	0.9646(3)	110.12(30)	2.69 ± 0.13^b
AgOH				
NR-SCF	2.101	0.943	120.8	1.14
NR-CCSD(T)	2.084	0.973	109.0	2.41
DK3-SCF	2.058	0.944	116.4	1.00
DK3-CCSD(T)	2.035	0.975	106.5	2.32
Exptl. ^a	2.01849(4)	0.9639(1)	107.81(2)	–
AuOH				
NR-SCF	2.161	0.943	119.2	1.02
NR-CCSD(T)	2.145	0.974	108.0	2.30
DK3-SCF	1.981	0.945	109.7	0.78
DK3-CCSD(T)	1.963	0.977	103.7	2.39

^a Ref. [38]; ^b Ref. [42]

correlation effect. The configuration interaction with singles and doubles (CISD) dissociation energies are reported as 2.68 eV [40] and 2.57 eV [41], which agree fairly well with the experimental value [42] of 2.69 ± 0.13 eV. On the other hand, the present results of 3.05 eV (NR-CCSD(T)) and 3.08 eV (DK3-CCSD(T)) are about 0.4 eV larger than the experimental value. However, *Bauschlicher* [39] stated in his paper that the CISD dissociation energy was likely to be underestimated by up to 0.5 eV and suggested that the correct value lies in the upper range of the experimental D_e . Our CCSD(T) results strongly support that the experimental D_e is too low.

Although the relativistic effect is small for CuOH, it contracts the Cu–OH bond length by 0.02 Å and the computed bond length comes closer to the experimental value. DK3-CCSD(T) yields a Cu–OH bond length of 1.774 Å, which is in excellent agreement with the experimental value [38] of 1.774182 Å. The relativistic effect is small for the bond angle and for the dissociation energy compared with the electron correlation effect. Relativity has little effect on the O–H bond length. This is true for AgOH and AuOH. The O–H bond lengths for these metal hydroxides calculated at the CCSD(T) level are 0.973–0.977 Å, while those at the SCF level are 0.943–0.945 Å.

The electron correlation effect for AgOH is again significant on the bond angle and the dissociation energy. The relativistic effect for AgOH is more significant than for CuOH. It contracts the Ag–OH bond length by 0.05 Å, while the electron correlation effect decreases it by 0.03 Å. The AgOH bond angle is reduced by 2–4°

with the inclusion of relativistic effects. Note that the relativistic effect decreases D_e of AgOH in contrast to that of CuOH and AuOH.

The relativistic effect for AuOH is the most significant among the three metal hydroxides. The relativistic effect decreases the Au–OH bond length by 0.20 Å, while the electron correlation effect reduces it by only 0.02 Å. The relativistic effect on the Au–OH bond length is ten times larger than the electron correlation effect. The AuOH bond angle is computed to be smaller than that of CuOH and AgOH. *Whitham et al.* argued that the decrease in the AgOH bond angle compared with that of CuOH may reflect the larger M –OH bond length. However, the decrease in the AuOH bond angle cannot be explained by their explanation since the Au–OH bond length is shorter than that for Ag–OH. The large decrease in the AuOH bond angle is mainly due to the relativistic effect. The electron correlation effect also reduces the bond angles of metal hydroxides.

The large relativistic change of the bond angle is interesting, since it has been generally believed that relativity has only a minor effect on the bond angle. The ionic character of the M –OH bond will increase the bond angle towards linearity, while the covalent character will decrease it towards nonlinearity as we can easily guess from covalent H₂O. The relativistic stability of the valence s orbital (0.09 eV for Cu, 0.27 eV for Ag, and 1.25 eV for Au at the SCF level) weakens the ionic character and strengthens the covalent character of the M –OH bond.

4.2. Electronic Structures of $M(\text{CO})_6$ ($M = \text{W}$ and Sg)

We have studied the valence photoelectron spectra of hexacarbonyl complexes of tungsten and seaborgium (element 106, Sg) theoretically [18]. Seaborgium is a transactinide element and is predicted to be a d-block transition element with six valence electrons as well as tungsten. In this study, we try to assign the photoelectron spectra of $\text{W}(\text{CO})_6$ and $\text{Sg}(\text{CO})_6$ using the relativistic PS method. While the experimental photoelectron spectra of $\text{W}(\text{CO})_6$ have been reported previously [43], no spectra have been reported for $\text{Sg}(\text{CO})_6$ unfortunately because Sg element is unstable and $\text{Sg}(\text{CO})_6$ has not been synthesized so far. Thus, the present calculations will give a useful knowledge of unknown $\text{Sg}(\text{CO})_6$ complex.

We used the finite-nucleus *Gaussian* basis sets [23s19p14d9f]/(7s5p4d2f) and [25s21p17d12f]/(8s6p5d3f) for W and Sg, respectively [44]. For carbon and oxygen we employed [12s8p1d]/(3s2p1d) sets taken from Ref. [45]. The contraction coefficients for C and O were determined by the atomic four-component SCF calculation. Their polarization functions are taken from 6-31G* sets. The C–O, W–C, and Sg–C bond lengths were set to 1.13, 2.06, and 2.15 Å, respectively, following *Nash and Bursten* [46]. Electron correlation effects were treated by the hybrid DFT approach with the B3LYP functional. In the computation of ionization potentials, we used the analog of *Koopmans'* theorem within DFT, that is, the estimation using *KS* eigenvalues, though the *Slater's* transition state method is available for better estimation of ionization potentials in our REL4D program. It is well known that the analog of *Koopmans'* theorem can reproduce experimental ionization potentials well by the adequate shift of the *KS* eigenvalues obtained. The fine grid was adopted in the PS calculation.

Table 5. Ionization potentials of $W(CO)_6$ calculated with PS-DFT (B3LYP)

PS-DFT				Exptl. ^a	
Assign (O_h^*) ^b	Assign (O_h) ^c	Nature ^d	IP/eV ^e	IP/eV	Assign
$e_{5/2}^+$	$2t_{2g}$	W5d + CO π	8.30	8.30	$2t_{2g}$
$g_{3/2}^+$	$2t_{2g}$	W5d + CO π	8.53	8.56	$2t_{2g}$
$g_{3/2}^-$	$8t_{1u}$	W5p + CO σ	13.13	13.27	$8t_{1u}$
$e_{1/2}^-$	$8t_{1u}$	W5p + CO σ	13.58	–	–
$g_{3/2}^+$	$1t_{1g}$	CO π	14.51	14.20	$1t_{1g}$
$e_{1/2}^+$	$1t_{1g}$	CO π	14.53	–	–
$e_{5/2}^-$	$1t_{2u}$	CO π	14.65	14.42	$1t_{2u}$
$g_{3/2}^-$	$1t_{2u}$	CO π	14.66	–	–
$g_{3/2}^-$	$7t_{1u}$	CO σ + W5p	14.84	} 14.88	–
$g_{3/2}^+$	$5e_g$	CO σ + W5d	14.94		$5e_g$
$e_{1/2}^-$	$7t_{1u}$	CO σ + W5p	14.95		–
$e_{5/2}^+$	$1t_{2g}$	CO π + W5d	15.06	15.2	$7t_{1u}$
$g_{3/2}^+$	$1t_{2g}$	CO π + W5d	15.08	–	–
$e_{1/2}^+$	$8a_{1g}$	W6s	15.74	15.54	$1t_{2g}$

^a Ref. [32]; ^b in the double group representations; ^c in the single group representations; ^d the mainly contributing orbital in each component is given to the head; ^e the computed values of the ionization energies are shifted by +1.5426 eV

The ionization potentials of $W(CO)_6$ are shown in Table 5 and Fig. 1. The valence photoelectron spectra of $W(CO)_6$ have been reported by *Higgenson et al.* [43]. The HeI photoelectron spectrum is also shown in Fig. 1. For the purposes of the direct comparison with experiment, the computed values of ionization energies were shifted by +1.5426 eV. It is found from Fig. 1 that the calculated ionization potentials are in good agreement with the experimental photoelectron spectrum. In Table 5, the orbital assignments of ionization are given in the O_h^* double group symmetry as well as the O_h single group. The first ionization band splits into two components with the separation of 0.23 eV by the spin-orbit splitting of the bonding orbitals between 5d of W and CO π orbitals. These two peaks are assigned to $e_{5/2}^+$ and $g_{3/2}^+$ in the double group representations split from the $2t_{2g}$ orbital in the single group symmetry. The obtained splitting value is in good agreement with the experimental finding (0.26 eV). The spin-orbit splitting of this band has been calculated by relativistic DV- $X\alpha$ method previously [46]. Our value is also in good agreement with the DV- $X\alpha$ value (0.23 eV). The peak around 13.0 eV can be assigned as the ionizations from $g_{3/2}^-$ and $e_{1/2}^-$ orbitals composed of W 5p and CO σ orbitals. Like the first band, this band also splits into two peaks due to the spin-orbit coupling of W 5p orbital, though such a splitting cannot be found in the experimental spectra. We can see the complicated overlapping bands in the region between 14.0 and 15.0 eV. These bands are mainly derived from the CO ionizations. Because of the small spin-orbit effect on CO, the spin-orbit splittings of $1t_{1g}$ and $1t_{2u}$ orbitals are negligibly small. These two peaks correspond with the experimental peaks around 14.20 and 14.42 eV, respectively. The overlapping ionization peaks appear around 14.9 eV. These peaks are due to ionizations from the CO

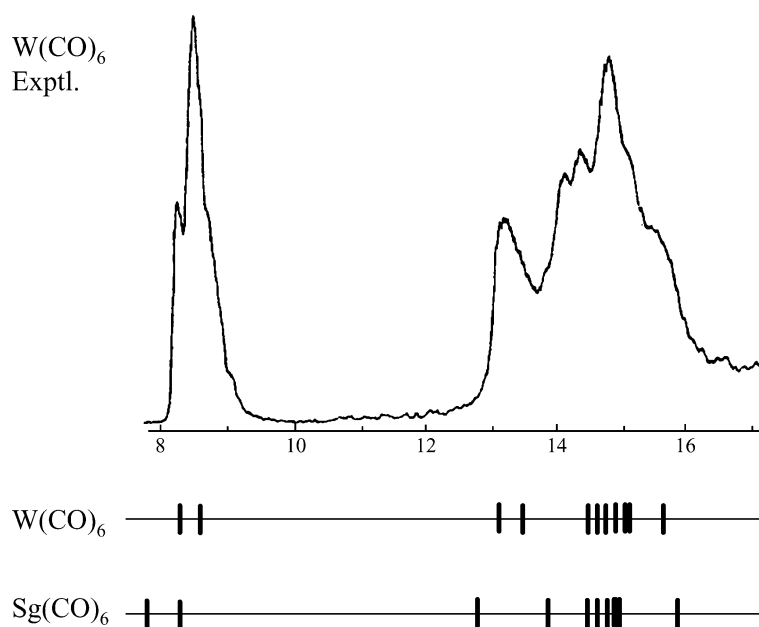


Fig. 1. The experimental HeI photoelectron spectrum of $\text{W}(\text{CO})_6$ and the calculated ionization potentials of $\text{W}(\text{CO})_6$ and $\text{Sg}(\text{CO})_6$

orbitals mixed slightly with the W 5p or 5d orbital. We assign the weak experimental peak around 15.54 eV to ionization from the $e_{1/2}^+$ ($8a_{1g}$) orbital composed mainly of W 6s orbital in contrast to the experimental assignment, $1t_{2g}$ orbital. We believe that the present assignments are more reliable, since the past experimental assignments are made with help of the $\text{Cr}(\text{CO})_6$ calculation of *Hillier and Saunders* in 1971 [47].

The ionization potentials of $\text{Sg}(\text{CO})_6$ are shown in Table 6. For the comparison with the ionization potentials of $\text{W}(\text{CO})_6$, the computed ionization potentials of $\text{Sg}(\text{CO})_6$ are also plotted in Fig. 1. In the case of $\text{Sg}(\text{CO})_6$, the corrected ionization potentials are estimated by shifting the calculated ionization energies by +1.4991 eV. This correction value is obtained by the consideration that the $1t_{1g}$ ionization peak of both $\text{W}(\text{CO})_6$ and $\text{Sg}(\text{CO})_6$ will be settled in the similar position because this peak mainly stems from the CO ionizations independent of metal atoms. It is expected that the photoelectron spectrum of $\text{Sg}(\text{CO})_6$ is similar to that of $\text{W}(\text{CO})_6$ from Fig. 1. Analogous to $\text{W}(\text{CO})_6$, the first two peaks assigned to $e_{5/2}^+$ and $g_{3/2}^+$ are due to the spin-orbit splitting of Sg 6d orbital mixed with CO π orbital. The calculated splitting is 0.44 eV and almost twice as large as that of $\text{W}(\text{CO})_6$ due to the larger spin-orbit effect. This value is in good agreement with DV-X α value (0.45 eV) by *Nash and Bursten* [46]. The next state also splits into two peaks with the large separation of 1.07 eV due to the spin-orbit coupling of Sg 6p orbital. The remaining peaks of $\text{Sg}(\text{CO})_6$ are almost similar to that of $\text{W}(\text{CO})_6$ because these states are mainly due to the CO ionizations. One major difference is the order of $e_{1/2}^-$ and $e_{5/2}^+$ states, which are derived from $7t_{1u}$ and $1t_{2g}$ in the single group representation. The reason for the switching is the larger spin-orbit effect of Sg p orbital on the $7t_{1u}$ state. The spin-orbit separations of the $7t_{1u}$ state are 0.11 and

Table 6. Ionization potentials of $\text{Sg}(\text{CO})_6$ calculated with PS-DFT (B3LYP)

PS-DFT			
Assign (O_h^*) ^a	Assign (O_h) ^b	Nature ^c	IP/eV ^d
$e_{5/2}^+$	$2t_{2g}$	Sg6d + CO π	7.85
$g_{3/2}^+$	$2t_{2g}$	Sg6d + CO π	8.29
$g_{3/2}^-$	$8t_{1u}$	Sg6p + CO σ	12.82
$e_{1/2}^-$	$8t_{1u}$	Sg6p + CO σ	13.89
$g_{3/2}^+$	$1t_{1g}$	CO π	14.51
$e_{1/2}^+$	$1t_{1g}$	CO π	14.52
$e_{5/2}^-$	$1t_{2u}$	CO π	14.62
$g_{3/2}^-$	$1t_{2u}$	CO π	14.63
$g_{3/2}^-$	$7t_{1u}$	CO σ + Sg6p	14.73
$g_{3/2}^+$	$5e_g$	CO σ + Sg6d	14.88
$e_{5/2}^+$	$1t_{2g}$	CO π + Sg6d	14.95
$e_{1/2}^-$	$7t_{1u}$	CO σ + Sg6p	14.95
$g_{3/2}^+$	$1t_{2g}$	CO π + Sg6d	14.99
$e_{1/2}^+$	$8a_{1g}$	Sg7s	15.92

^a In the double group representations; ^b in the single group representations; ^c the mainly contributing orbital in each component is given to the head; ^d the computed values of the ionization energies are shifted by +1.4991 eV

0.22 eV for $\text{W}(\text{CO})_6$ and $\text{Sg}(\text{CO})_6$, respectively. The $e_{1/2}^+$ state originated from $8a_{1g}$ of $\text{Sg}(\text{CO})_6$ (15.92 eV) appears in the higher energy position than that of $\text{W}(\text{CO})_6$ (15.74 eV). This is due to the larger relativistic stabilization of the s orbital of Sg.

4.3. Theoretical Studies on the Course of CO Insertion into Pt–C and Pd–C Bonds in Cationic Complexes

The CO insertion into a transition metal-carbon bond constitutes one of the most essential elementary processes in transition metal-catalyzed carbonylation of organic compounds [48–50]. Palladium complexes have been utilized most extensively in the carbonylations of aryl and vinyl halides as well as of olefins besides cobalt and rhodium complexes. In the palladium-catalyzed carbonylation, generation of a cationic catalytic species has been often found to enhance the catalytic activities. Recently, behavior of neutral and cationic *cis*- and *trans*-monoorganoplatinum complexes has been examined and compared with that of the corresponding monoorganopalladium complexes experimentally [51]. Treatment of the cationic Pt complexes with CO gave no CO insertion product but afforded only the CO-coordinated *trans*-monoorganoplatinum complexes. The reluctance of the organoplatinum complexes toward CO insertion stands in contrast with the ease for the CO insertion of the corresponding organopalladium complexes. For clarifying the reasons of the marked difference between the behaviors of the two Group 10 metal complexes the theoretical study has been performed [51].

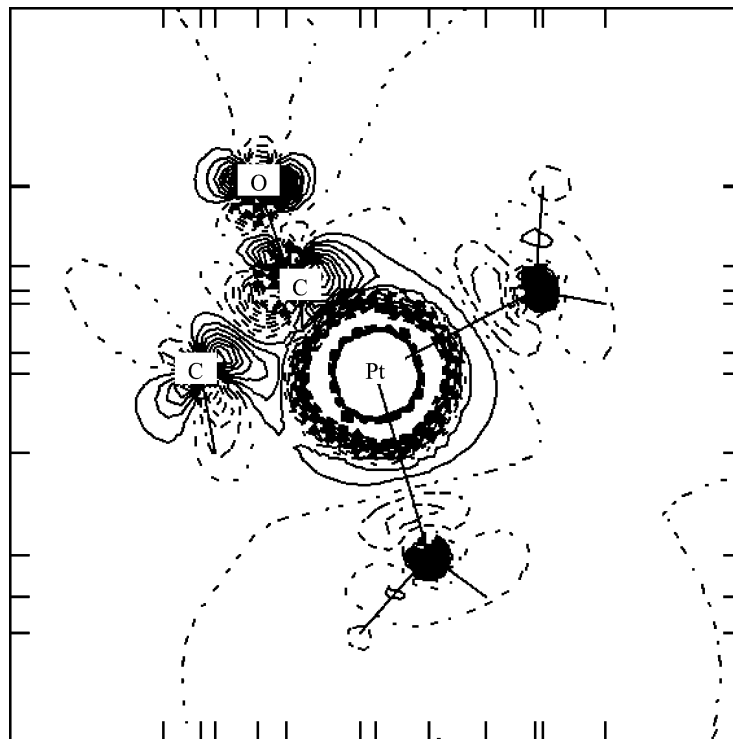
As the relativistic effect is much larger in the Pt complex than the Pd complex, it is expected that the relativistic effect can explain the difference of the reactivity

Table 7. Non-relativistic (NR) and relativistic (Rel.) results of activation energy and heat of formation in the CO insertion to the Pt complex (in kcal/mol)

	Reactant	TS	Product
NR	0.0	20.6	-1.5
Rel.	0.0	33.2	20.9

between both complexes. Thus, we investigated the relativistic effect on the CO insertion reaction in the Pt complex. The RESC theory was used for this purpose.

Table 7 shows non-relativistic and relativistic results of the activation energy and the heat of formation in the CO insertion reaction to the Pt complex. The activation energy increases and this reaction becomes endothermic with the relativity. That is, the relativistic effect affects to arrest the CO insertion in the Pt complex. This agrees with the fact that this reaction does not occur in the Pt complex. The remarkable effect with the relativity appears in the transition state of this reaction. Figure 2 shows the density difference between the relativistic and non-relativistic densities in the transition state. The density around the Pt atom decreases spherically by the relativistic effect due to the well-known contraction of the *s* atomic orbital with the relativity. In addition, this density difference map shows that it becomes unfavorable to form the C–C bonding with the relativity.

**Fig. 2.** Density difference between the relativistic and non-relativistic densities in the transition state of the CO insertion to the Pt complex

This is interesting because the relativistic effect of the heavy Pt atom can affect the distant bonding formation between light C atoms.

5. Summary

The recent developments of our relativistic molecular theories are introduced in this review. Our approaches are expected to be useful and effective for various studies of electronic structures and spectroscopic properties of large-scale heavy-element systems.

Acknowledgements

This research was supported in part by a grant-in-aid for Scientific Research in Specially Promoted Research "Simulations and Dynamics for Real Systems" and the Grant for 21st Century COE Program "Human-Friendly Materials based on Chemistry" from the Ministry of Education, Science, Culture, and Sports of Japan, and by a grant from the Genesis Research Institute.

References

- [1] Nakajima T, Yanai T, Hirao K (2002) *J Comp Chem* **23**: 847
- [2] Yanai T, Nakajima T, Ishikawa Y, Hirao K (2004) In: Hirao K, Ishikawa Y (eds) *Recent Advances in Relativistic Effects in Chemistry*. World Scientific, Singapore, p 221
- [3] Nakajima T (2003) *Bull Korean Chem Soc* **24**: 809
- [4] Ishikawa Y, Koc K (1997) *Phys Rev A* **56**: 1295; Vilkas MJ, Ishikawa Y, Koc K (1998) *Phys Rev E* **58**: 5096; Vilkas MJ, Ishikawa Y, Hirao K (2000) *Chem Phys Lett* **321**: 243
- [5] Eliav E, Kaldor U, Ishikawa Y (1996) *Phys Rev A* **53**: 3050
- [6] Visscher L, Visser O, Aerts H, Merenga H, Nieuwpoort WC (1994) *Comput Phys Commun* **81**: 120
- [7] Saue T, Fægri K, Helgaker T, Gropen O (1997) *Mol Phys* **91**: 937
- [8] Quiney HM, Skaane H, Grant IP (1999) *Adv Quantum Chem* **32**: 1; Grant IP, Quiney HM (2000) *Int J Quant Chem* **80**: 283
- [9] Mohanty A, Clementi E (1991) *Int J Quant Chem* **39**: 487
- [10] Pisani L, Clementi E (1994) *J Comput Chem* **15**: 466
- [11] Dylla KG, Taylor PR, Fægri K, Partridge H (1991) *J Chem Phys* **95**: 2583
- [12] Ishikawa Y, Binning RC, Sando KM (1983) *Chem Phys Lett* **101**: 111; Stanton RE, Havriliak S (1984) *J Chem Phys* **81**: 1910
- [13] Yanai T, Nakajima T, Ishikawa Y, Hirao K (2001) *J Chem Phys* **114**: 6525
- [14] Yanai T, Iikura H, Nakajima T, Ishikawa Y, Hirao K (2001) *J Chem Phys* **115**: 8267
- [15] Yanai T, Nakajima T, Ishikawa Y, Hirao K (2002) *J Chem Phys* **116**: 10122
- [16] Head-Gordon M, Pople JA (1988) *J Chem Phys* **89**: 5777
- [17] Ishida K (1996) *Int J Quant Chem* **59**: 209; Ishida K (1998) *J Chem Phys* **109**: 881; Ishida K (1998) *J Comput Chem* **19**: 923; Ishida K (1999) *J Chem Phys* **111**: 4913
- [18] Nakajima T, Hirao K (2004) *J Chem Phys* **121**: 3438
- [19] Friesner RA (1985) *Chem Phys Lett* **116**: 39
- [20] Friesner RA (1986) *J Chem Phys* **85**: 1462
- [21] Huber KP, Herzberg G (1979) *Molecular Structure IV, Constants of Diatomic Molecules*. Van Nostrand, New York
- [22] Simard B, Hackett PA (1990) *J Mol Spectrosc* **412**: 310
- [23] Bethe HA, Salpeter EE (1957) *Quantum Mechanics of One- and Two-Electron Atoms*. Springer, Berlin Heidelberg New York

- [24] Foldy LL, Wouthuysen SA (1950) *Phys Rev* **78**: 29
- [25] van Lenthe E, Baerends EJ, Snijders JG (1993) *J Chem Phys* **99**: 4597
- [26] Chang Ch, Pelissier M, Durand Ph (1986) *Phys Scr* **34**: 394
- [27] Kutzelnigg W (1989) *Z Phys D* **11**: 15
- [28] Kutzelnigg W (1990) *Z Phys D* **15**: 27
- [29] Dyall KG (1994) *J Chem Phys* **100**: 2118
- [30] Nakajima T, Hirao K (1999) *Chem Phys Lett* **302**: 383
- [31] Nakajima T, Suzumura T, Hirao K (1999) *Chem Phys Lett* **304**: 271
- [32] Fedorov D, Nakajima T, Hirao K (2001) *Chem Phys Lett* **335**: 183
- [33] Nakajima T, Hirao K (2000) *J Chem Phys* **113**: 7786
- [34] Nakajima T, Hirao K (2000) *Chem Phys Lett* **329**: 511
- [35] Nakajima T, Hirao K (2003) *J Chem Phys* **119**: 4105
- [36] Douglas M, Kroll NM (1974) *Ann Phys NY* **82**: 89
- [37] Hess BA (1986) *Phys Rev A* **33**: 3742; Jansen G, Hess BA (1989) *ibid* **39**: 6016
- [38] Whitham CJ, Ozeki H, Saito S (1999) *J Chem Phys* **110**: 11109; Whitham CJ, Ozeki H, Saito S (2000) *J Chem Phys* **112**: 641
- [39] Ikeda S, Nakajima T, Hirao K (2003) *Mol Phys* **101**: 105
- [40] Bauschlicher CW (1986) *Int J Quant Chem* **S20**: 563
- [41] Mochizuki Y, Takada T, Murakami A (1991) *Chem Phys Lett* **185**: 535
- [42] Belyaer VN (1978) *Izv Vyssh Uchebn Zaved Khim Khim Tekhnol* **21**: 1968
- [43] Higgenson BR, Lloyd DR, Burroughs P, Gibson DM, Orchard AF (1973) *J Chem Soc Faraday Trans 2*, **69**: 1659
- [44] Faegri K (2001) *Theor Chem Acc* **105**: 252
- [45] Nakajima T, Hirao K (2002) *J Chem Phys* **116**: 8270
- [46] Nash CS, Bursten BE (1995) *New J Chem* **19**: 669
- [47] Hillier IH, Saunders VR (1971) *Mol Phys* **22**: 1025
- [48] Tsuji J (1995) *Palladium Reagents and Catalysts Innovations in Organic Synthesis*. Wiley, Chichester
- [49] Heck RF (1985) *Palladium Reagents in Organic Syntheses*. Academic Press, New York
- [50] Beller M (1996) In: Cornils B, Herrmann WA (eds) *Applied Homogeneous Catalysis with Organometallic Compounds*. VCH, Weinheim, vol 1, p 148
- [51] Kayaki Y, Tsukamoto H, Kaneko M, Shimizu I, Yamamoto A, Tachikawa M, Nakajima T (2001) *J Organometallic Chem* **622**: 199